Hydrodynamic entropy and emergence of order in two-dimensional Euler turbulence

Mahendra K. Verma ●* and Soumyadeep Chatterjee ●†
Department of Physics, Indian Institute of Technology Kanpur, Kanpur 208016, India

Using numerical simulations, we show that the asymptotic states of two-dimensional (2D) Euler turbulence exhibit large-scale flow structures due to nonzero energy transfers among small wavenumber modes. These asymptotic states, which depend on the initial conditions, are out of equilibrium, and they are different from the predictions of Onsager and Kraichnan. We propose "hydrodynamic entropy" to quantify order in 2D Euler turbulence; we show that this entropy decreases with time, even though the system is isolated with no dissipation and no contact with a heat bath.

I. INTRODUCTION

Euler turbulence remains unsolved till date. In this paper, we address the energy flux and entropy of two-dimensional (2D) Euler turbulence. The equations of incompressible Euler flow are

$$\partial_t \mathbf{u} + \mathbf{u} \cdot \boldsymbol{\nabla} \mathbf{u} = -\boldsymbol{\nabla} p; \quad \boldsymbol{\nabla} \cdot \mathbf{u} = 0, \tag{1}$$

where $\mathbf{u}$, p are the velocity and pressure fields, respectively [1,2]. The above system is *isolated*, as it lacks external force and viscous dissipation. Consequently, the thermodynamic entropy of an Euler flow remains constant [1]. However, when we solve Euler equations with an ordered initial condition, structurally, three-dimensional (3D) Euler turbulence becomes more random during its evolution [3], whereas 2D Euler turbulence tends to become more orderly [4,5]. Hence, the entropy of Euler turbulence needs a reexamination.

Onsager [6] modeled 2D Euler flow using a collection of point vortices interacting via logarithmic potential. Onsager showed that for large energy, 2D Euler turbulence exhibits negative temperature and a large cluster of same-circulation vortices. Recently, Gauthier *et al.* [7] observed such giant vortices in an experiment involving 2D quantum fluid, thus providing an experimental verification of Onsager's theory. Billam *et al.* [8] developed a first-principles realization of Onsager's vortex model in a 2D superfluid. Miller [9] and Robert [10] extended Onsager's theory to continuum version of 2D Euler turbulence and computed entropy for the flow. Using tools of equilibrium statistical mechanics, Bouchet and Simonnet [11], and Bouchet and Venaille [12] derived multiple stationary states, namely, a dipole and unidirectional flow (shear layer), for 2D Euler turbulence. Pakter and Levin [13] provided a contrary viewpoint and showed that 2D Euler turbulence is out of equilibrium and that a system of interacting vortices becomes trapped in a nonequilibrium stationary state; these results deviate from the predictions of Onsager [6]. Refer to review articles by Eyink and Sreenivasan [14], and Bouchet and Venaille [12] for an extensive discussion.

---

*mkv@iitk.ac.in
†inspire.soumya@gmail.com

Lee [15] and Kraichnan [16] provide an alternative framework for Euler turbulence. They showed that the evolution of Fourier modes of Euler equation follows Liouville's theorem, and that the equilibrium solutions of Euler turbulence are

$$E(k) = \frac{k^2}{\beta - \gamma k^2} \quad \text{for 3D,} \tag{2}$$

$$E(k) = \frac{k}{\beta + \gamma k^2} \quad \text{for 2D,} \tag{3}$$

where β and γ are constants. Here, the Fourier modes form a microcanonical ensemble. The derivation of Eqs. (2) and (3) involves two competing conservation laws: kinetic energy ($\int d\mathbf{r} u^2/2$) and kinetic helicity ($\int d\mathbf{r}(\mathbf{u} \cdot \boldsymbol{\omega})$) in 3D, and kinetic energy and enstrophy ($\int d\mathbf{r} \omega^2/2$) in 2D, where $\boldsymbol{\omega}$ is the vorticity field. For some combinations of energy and enstrophy, 2D Euler turbulence yields $\beta < 0$ or negative temperature [4,17]. Kraichnan and Montgomery [17] provide a detailed review of 2D Euler turbulence.

For a δ-correlated random velocity field as an initial condition, both 2D and 3D Euler turbulence follow the energy spectra of Eqs. (2) and (3) with $\gamma \approx 0$ [18,19]. In addition, for an initial condition with large-scale structures, 3D Euler turbulence asymptotes to $E(k)$ of Eq. (2) [3]. However, $E(k)$ of 2D Euler turbulence differs from Eq. (3) for coherent velocity field as an initial condition. For example, for enstrophy-dominated 2D Euler turbulence, Fox and Orszag [4] reported deviations from Eq. (3) at small wave numbers. For parameters where $\beta + \gamma k^2 \approx 0$, Seyler *et al.* [5] observed large vortex structures, similar to those in a discrete vortex system [20]. Dritschel *et al.* [21] studied the unsteady nature of 2D flow structures on a sphere. Robert and Sommeria [22] and Bouchet and Venaille [12] analyzed such structures in the framework of equilibrium statistical mechanics.

The works of Fox and Orszag [4], Seyler *et al.* [5], Pakter and Levin [13], Bouchet and Simonnet [11], Dritschel *et al.* [21], and Modin and Viviani [23] indicate that 2D Euler turbulence is out of equilibrium, contrary to the assumptions of Onsager [6] and Kraichnan [16]. Bouchet and Venaille [12] argued that even though nonequilibrium steady states of 2D Euler turbulence often break detailed balance, under weak force and zero viscosity, they may be described by microcanonical measures and entropy functional. Bouchet and coworkers [11,12,24], and Modin and Viviani [23] explained the structures of 2D Euler turbulence in this framework. In this paper, we advance this theme by carefully examining the energy transfers and energy flux of 2D Euler turbulence. We show that the small wave-number modes exhibit nonzero energy transfers and hence break the *detailed balance*, which is a stringent criterion for equilibrium. Thus, we demonstrate the nonequilibrium nature of 2D Euler turbulence. We also quantify the order of the structures using hydrodynamic entropy.

The outline of the paper is as follows. In Sec. II, we describe the nonequilibrium nature of 2D Euler turbulence. We propose hydrodynamic entropy in Sec. III to quantify this nature. We conclude the paper in Sec. IV.

II. NONEQUILIBRIUM NATURE OF 2D EULER TURBULENCE

Prior to a detailed discussion on 2D Euler turbulence, we summarize the energy spectrum and flux of 3D Euler turbulence. Cichowlas *et al.* [3] simulated 3D Euler turbulence with Taylor-Green vortex as an initial condition. For such simulations, in the early phase, the energy flows from large scales to small scales and the energy flux is positive. After several eddy turnover times, the system approaches equilibrium with vanishing energy flux. Refer to the Appendix for details.

For 2D Euler turbulence, we performed pseudospectral simulations on a $(2\pi)^2$ box with a M^2 grid. Here, $M = 512$. We dealiase the code by setting all the modes outside the sphere of radius $M/3$ to zero. To conserve the total energy, we time evolve Eqs. (1) using the *position-extended Forest-Ruth-like* (PEFRL) scheme [25,26] with time step $= 10^{-4}$. We carried out three runs with the following initial conditions:
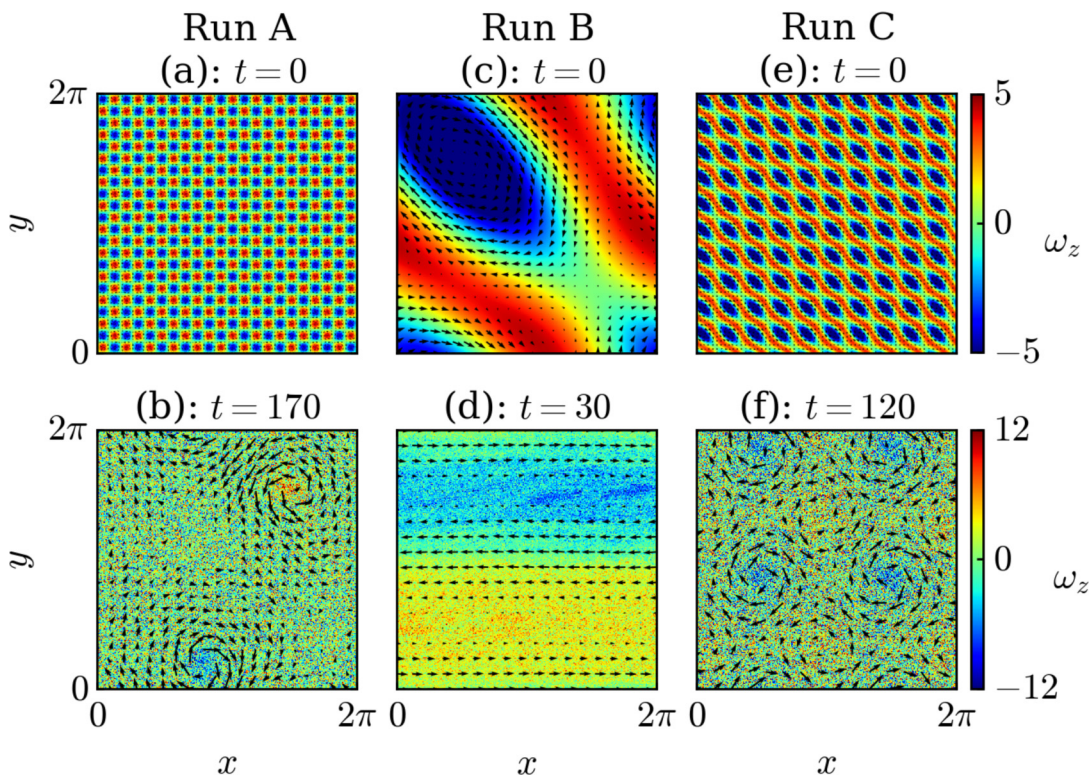
FIG. 1. For runs A–C of 2D Euler turbulence: (a), (c), (e) the initial states (b), (d), (f) the final states, respectively. Here we plot the velocity field over the density plots of the vorticity field.

(1) Run A: The initial velocity profile is taken as $(\sin 11x \cos 11y + \eta_x, -\cos 11x \sin 11y + \eta_y)$, where (η_x, η_y) is random noise. We take $|\eta_x| \ll 1$ and $|\eta_y| \ll 1$.

(2) Run B: The initial nonzero velocity Fourier modes are $\mathbf{u}(1, 0) = (0, 1)$, $\mathbf{u}(0, 1) = (1, 0)$, and $\mathbf{u}(1, 1) = (-i, i)$.

(3) Run C: The initial nonzero velocity Fourier modes are $\mathbf{u}(10, 0) = (0, 1)$, $\mathbf{u}(0, 10) = (1, 0)$, and $\mathbf{u}(10, 10) = (-i, i)$.

We time advance runs A, B, C up to 170, 30, and 120 turnover times $(2\pi/U_{\rm rms})$ respectively. We observe runs B and C reach the steady flow profiles after 10 to 20 eddy turnover times, whereas run A reaches the steady state after 100 eddy turnover times. We label these states *asymptotic states*. In this paper, we show that these states are out of equilibrium. The dependence of the asymptotic states on the initial condition is consistent with earlier works, e.g., Celani *et al.* [27]. The top and bottom panels of Fig. 1 illustrate, respectively, the initial and asymptotic states of the three runs. Here, the velocity field is superposed over the density plots of the vorticity field. Runs A–C asymptote, respectively, to a vortex-antivortex pair [6], a unidirectional flow (shear layer), and four vortex-antivortex pairs. The above large-scale flow structures are embedded in small-scale noisy flow. Similar structures have been observed by Bouchet and Simonnet [11] and Dritschel *et al.* [21].

For Runs A–C, total energy $E = \int d\mathbf{r}(u^2/2)/\int d\mathbf{r} = 0.2500954, 4, 4$, while total enstrophy $\Omega = \int d\mathbf{r}(\omega^2/2)/\int d\mathbf{r} = 62.17, 6, 600$, respectively; and these quantities are conserved. For validation of our numerical codes, we plot the time series of the total energy and total enstrophy along with their relative errors in Figs. 2 and 3. The relative errors for energy and enstrophy are defined as

$$\epsilon(t) = \frac{|E(t) - E(t = 0)|}{E(t = 0)}; \quad \epsilon_\Omega(t) = \frac{|\Omega(t) - \Omega(t = 0)|}{\Omega(t = 0)}. \tag{4}$$
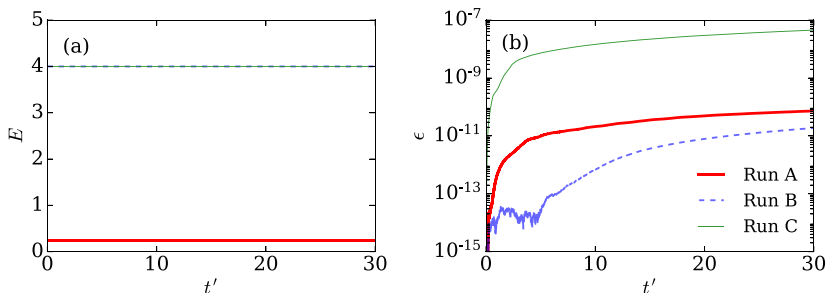
FIG. 2. (a) For runs A–C of 2D Euler turbulence, (a) time series of the total energy, E, and (b) its relative error, ϵ. We employ normalized time $t' = 3t/17, t, t/4$ for the three runs.

Since the three runs take different amounts of time to reach their respective asymptotic states, in the plots, we employ normalized time, $t' = 3t/17, t, t/4$, for runs A–C, respectively. For the asymptotic states of runs A–C, the relative errors in energy (ϵ) are 7.3×10^{-11}, 1.9×10^{-11}, and 4.5×10^{-8}, respectively, while those in entropy (ϵ_Ω) are 6.3×10^{-9}, 2.7×10^{-7}, and 6.5×10^{-6} respectively.

In Figs. 4(a) and 4(b), we plot the averaged energy spectra and fluxes of the three runs. Here, we average 6500, 1000, and 10000 frames of runs A–C in the respective time intervals (105, 170), (20, 30), and (20, 120). For intermediate and large wave numbers, $E(k)$ of the three runs follow Kraichnan's predictions [Eq. (3)]:

$$\text{Run A} : E(k) = \frac{k}{-3230 + 237k^2} \quad \text{for } k > 10, \tag{5}$$

$$\text{Run B} : E(k) = \frac{k}{-6357840 + 9361k^2} \quad \text{for } k > 40, \tag{6}$$

$$\text{Run C} : E(k) = \frac{k}{888 + 26k^2} \quad \text{for } k > 10, \tag{7}$$

with constants having significant errors. We construct these functions using *nonlinear least-squares fits* of the numerical data of $k/E(k)$ to $\beta + \gamma k^2$. We employ the standard *scipy.optimize.curve_fit* function of Python for the computation.

Based on Eqs. (5)–(7) and Fig. 4(a), we claim that the large wave-number modes are in equilibrium. Fjørtoft [28] and Nazarenko [29] showed that for 2D hydrodynamic turbulence, $k_E \leqslant \sqrt{\Omega/E} \leqslant k_\Omega$, where k_E and k_Ω are the centroids of energy and enstrophy respectively. For runs A–C, $\sqrt{\Omega/E} = 15.8, 1.2, 12.2$. Hence, the wave numbers far beyond k_Ω are dominated by enstrophy. In this regime, our simulations reveal that $E(k) \propto k^{-1}$, which corresponds to an
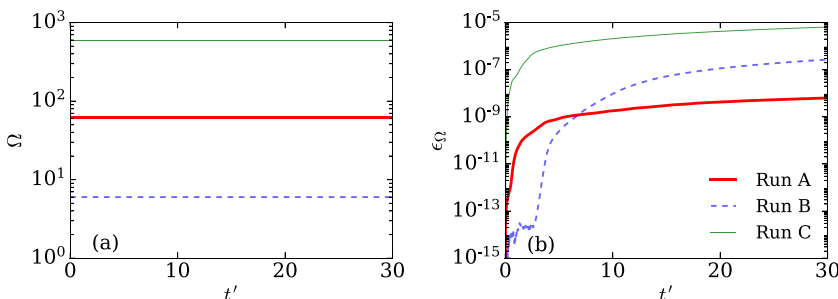

FIG. 3. For runs A–C of 2D Euler turbulence, (a) time series of total enstrophy, Ω, and (b) its relative error, ϵ_Ω, as a function of t', where $t' = 3t/17, t, t/4$ for the three runs.
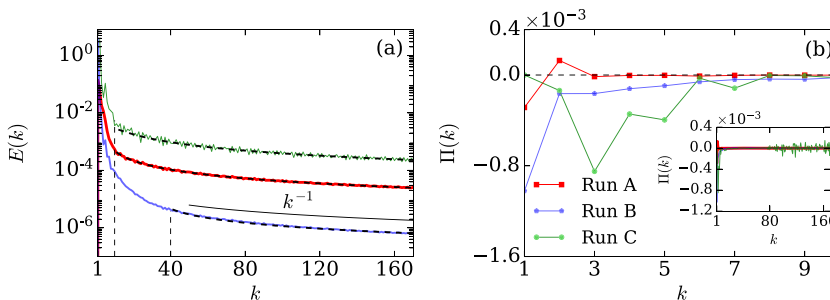
FIG. 4. For runs A–C of 2D Euler turbulence: plots of the averaged energy spectra, $E(k)$, and fluxes, $\Pi(k)$, of the asymptotic states. In (a), the best-fit curves of Eqs. (5)–(7) are shown as dashed curves. (b) exhibits $\Pi(k)$ for small k's, while inset shows $\Pi(k)$ for the whole range.

equipartition of enstrophy. That is, modal enstrophy, $E_\omega(\mathbf{k}) = E(\mathbf{k})k^2 = \text{const}$, which leads to $E(k) \sim 2\pi k/k^2 \sim k^{-1}$. Moreover, runs A and B exhibit $\beta < 0$ or negative temperature [6,16,17], which is related to the emergence of large scale structures. Note that Onsager [6] and Kraichnan [16] assumed the 2D Euler flow to be in equilibrium.

Equations (5)–(7) and Fig. 4(a) reveal that the small wave-number modes deviate strongly from Kraichnan's predictions for equilibrium Euler turbulence, consistent with the works of Fox and Orszag [4]. In the following discussion, we will show that the small-wave-number modes of 2D Euler are out of equilibrium from various perspectives. As illustrated in Fig. 5, for small wave numbers, $E(k)$'s do not follow $k^{-5/3}$ energy spectrum, except for a small range of wave numbers for run A. This is expected because Euler turbulence is very different from 2D hydrodynamic turbulence, which exhibits $E(k) \propto k^{-5/3}$ when the intermediate scales are forced [30].

We complement the spectral studies with a quantification of energy transfers and fluxes. Euler turbulence lacks external forcing and dissipation, hence the temporal evolution of $E(k)$ is given by [2,31–34]

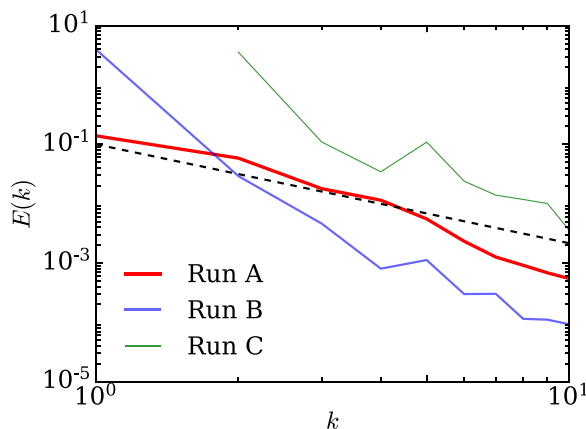$$\frac{dE(k,t)}{dt} = T(k,t), \tag{8}$$

FIG. 5. For runs A–C of 2D Euler turbulence, plots of the averaged energy spectra for small wave numbers $k \in [1, 10]$. The black-dashed line represents $k^{-5/3}$ spectrum. Clearly, runs B and C do not exhibit $k^{-5/3}$ spectrum, while run A matches with $k^{-5/3}$ for very small region.
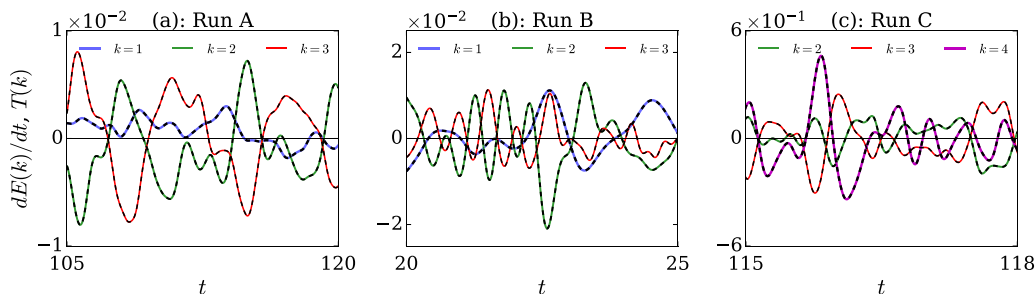
FIG. 6. For runs A–C, plots of the time evolutions of $dE(k)/dt$ (solid lines) and $T(k)$ (dashed lines) for three different wave numbers.

where $T(k, t)$ is the nonlinear energy transfer to wave-number shell k. If Euler turbulence were to be in equilibrium, then for all k's, $dE(k, t)/dt = 0$, implying that $T(k, t) = 0$. Consequently, the energy flux, $\Pi(k, t) = -\int_0^k T(k', t) dk'$ would vanish for all wave-number spheres. This test is an alternative one to the entropy maximization principle [33]. Energy conserving systems, as well as Hamiltonian systems, are expected to approach equilibrium asymptotically [31,35]. It has been shown that 3D Euler turbulence asymptotically reaches the equilibrium state with zero energy flux [3]. But we show below that $T(k, t)$ and $\Pi(k, t)$ for 2D Euler turbulence are nonzero for small k's, thus 2D Euler turbulence is out of equilibrium.

For 2D Euler turbulence, we illustrate $T(k, t)$ for the dominant wave-number shells ($k = 1$ to 4) in Fig. 6. Clearly, these $T(k, t)$'s fluctuate significantly, and $dE(k, t)/dt \approx T(k, t)$, thus validating Eq. (8). For small k's, the nonzero $T(k, t)$'s yield negative energy flux. In particular, $\min[\langle \Pi(k) \rangle] \approx -3 \times 10^{-4}, -10^{-3}, -8.4 \times 10^{-4}$ for runs A–C, respectively. Note that the finite $T(k, t)$ and $\Pi(k, t)$ for 2D turbulence are much larger than the corresponding quantities of 3D Euler turbulence (see the Appendix). The nonzero $T(k, t)$ and $\Pi(k, t)$ break the *detailed balance of energy transfers* and indicate nonequilibrium nature of 2D Euler turbulence.

Based on the above observations, we conclude that the intermediate and large wave-number shells are in equilibrium but the small wave-number shells are out of equilibrium. However, there is an exception to the above rule. For the δ-correlated velocity field as an initial condition, 2D Euler turbulence exhibits equilibrium solution with $E(k) \propto k$ [19]. For this particular case, $\gamma \approx 0$, and k_Ω exceeds the grid size.

In classical literature of hydrodynamics, the thermodynamic entropy of Euler turbulence is taken to be constant [1]. However, as discussed above, the disorder in Euler turbulence varies with time. Hence, the thermodynamic entropy cannot capture the disorder in Euler turbulence. In Sec. III, we define hydrodynamic entropy, which can describe the disorder in Euler turbulence.

III. HYDRODYNAMIC ENTROPY

Consider two gaseous systems shown in Fig. 7. In Fig. 7(a), the molecules are in thermal equilibrium, and they move randomly with thermal speed C_s. Thermodynamic entropy provides a good measure for the disorder in such a system.

In Fig. 7(b), the molecules comove in a hydrodynamic vortex. This system is out of equilibrium because 2D hydrodynamic vortices coalesce to form large vortices via inverse cascade of energy. To quantify disorder in an hydrodynamic flow, we scale separate the microscopic thermal processes and the macroscopic fluid processes, and define two different entropies for them [18,36]. Thermodynamic entropy is employed for the microscopic processes [37,38], whereas hydrodynamic entropy, to be defined below, for describing macroscopic order. For Euler flow, only hydrodynamic entropy would be meaningful because thermodynamic entropy is zero for this case.
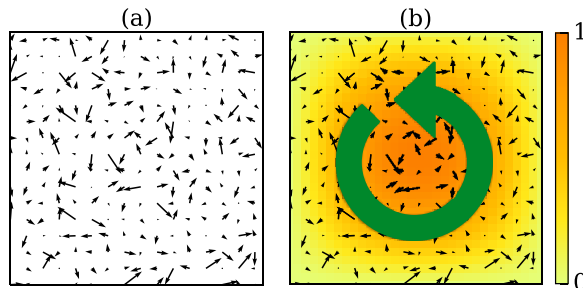
FIG. 7. (a) In a 2D gas in thermal equilibrium, the molecules move randomly with the sound speed C_s. (b) A schematic diagram illustrating the velocities of molecules in a hydrodynamic vortex.

We employ *Shannon entropy* [39] to quantify the disorder of the fluid structures at macroscopic level. For the same, we postulate that the probability of occurrence of a Fourier mode with wave number $\mathbf{k}$ is $p_{\mathbf{k}} = E(\mathbf{k})/E$, where $E(\mathbf{k})$ is the modal energy, and E is the total energy. Now the hydrodynamic entropy of the flow is defined as

$$S = -\sum_{\mathbf{k}} p_{\mathbf{k}} \log_2(p_{\mathbf{k}}). \tag{9}$$

The above entropy, which is defined for a snapshot, can be applied to any fluid flow. Note that hydrodynamic entropy is very different from thermodynamic entropy, which depends on temperature and volume of the system. At present, it is not apparent if hydrodynamic entropy and thermodynamic entropy could be put on a similar footing. It would be interesting to explore whether we can relate the two in a way Landauer [40] connected computation to entropy.

It is important to keep in mind that Shannon entropy [Eq. (9)] has been used earlier to quantify order in images, music, messages, and DNA, as well as in a variety of flow phenomena, e.g., boundary layers, transitions, etc. [41]. There are many other measures of entropy. For example, Clark *et al.* [42] employed Kolmogorov-Sinai entropy for quantifying 2D hydrodynamic flow, whereas Drivas and Elgindi [43] quantified entropy of Euler flow in terms of accessible phase space.

Euler flow is an ideal case where thermal processes are ignored (due to zero viscosity). Therefore, Euler flow has only hydrodynamic entropy. The entropies of the vortex solutions of Onsager [6] and Miller [9] are hydrodynamic, however, these measures may differ from those computed using Eq. (9). Interestingly, Kraichnan's equilibrium solution with $\gamma = 0$ corresponds to a δ–correlated velocity field [15,16,18]. For such a flow, $p_{\mathbf{k}} = 1/M$ and the hydrodynamic entropy $S = \log_2(M)$, where M is the number of modes of the system; this is the maximum possible hydrodynamic entropy for a flow with M degrees of freedom.

Before reporting the hydrodynamic entropy of 2D Euler turbulence, we describe the hydrodynamic entropy of 3D Euler turbulence. For the 3D Euler flow described in the Appendix, we compute the entropy using Eq. (9) and plot its time series in Fig. 8. We derive the functional dependencies of $S(t)$ using the nonlinear least-squares method. In the initial phase, the hydrodynamic entropy increases exponentially, after which it approaches the maximum possible value $S = \log_2(M) = 18.3$, where $M = (4\pi/3)(128/3)^3$ is the number of modes of the system. We observe that for 3D Euler turbulence, the approach to equilibrium is slow. Since S increases monotonically in time, we claim that 3D Euler turbulence evolves from order to disorder.

Now we compute the hydrodynamic entropies of the 2D Euler flows of runs A–C and plot the entropy time series in Fig. 9. The duration and timescales of the three runs are quite different. Hence, for a proper comparison, we normalize the time appropriately, i.e., $t' = 3t/17, t, t/4$ for runs A–C, respectively. We observe that for each case, the entropy fluctuates in the early stages, after which it decreases exponentially to an asymptotic value. Here too, we employ the nonlinear least-squares method to derive the functions that describe the decrease in S. The asymptotic entropies for
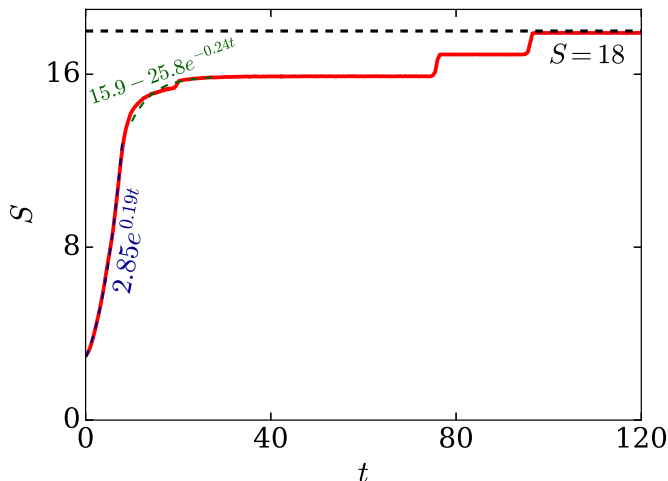
FIG. 8. In 3D Euler turbulence, hydrodynamic entropy exhibits monotonic growth, with an exponential increase in the beginning and saturation in the end.

runs A–C are 4.9, 1.2, and 3.1, respectively. These values are smaller than the maximum possible value, which is $\log_2(M) \approx 16.5$, where $M = \pi(512/3)^2$ is the number of active dealiased modes. Note, however, that S for all the runs exhibit small fluctuations in the asymptotic regime due to the dynamic nature of the flow. Recall the temporal fluctuations of $T(k, t)$ and $E(k, t)$ described in Sec. II. It is also important to note that the evolution of hydrodynamic entropy for 2D Euler turbulence is very different that of 3D Euler turbulence.

The asymptotic state of run B is the most ordered one (having least entropy) among the three runs. In the asymptotic regime of run B, the Fourier modes $\mathbf{u}(0, \pm 1)$ contains 99% of the total energy, hence, their probabilities are approximately $1/2$ each. Therefore, these two modes yield $S \approx \log_2(2) = 1$, while the other modes contribute the rest (0.2). To quantify the evolution of these modes, in Fig. 10, we plot the time series of $\mathrm{Re}[u_x(0, 1)]$ and $\mathrm{Im}[u_x(0, 1)]$ of run B. As shown in
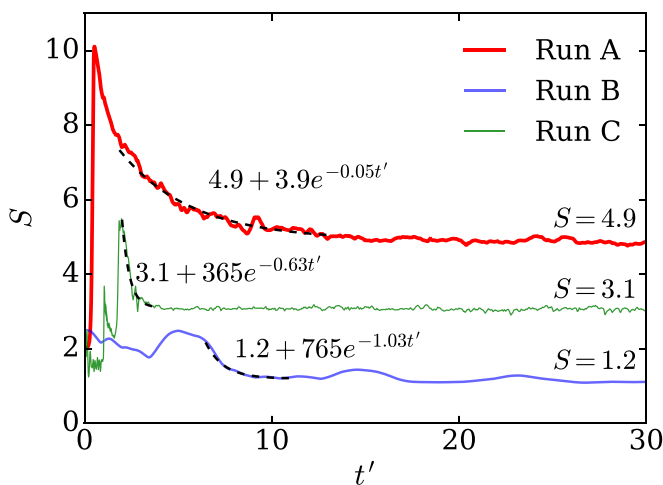

FIG. 9. For runs A–C of 2D Euler turbulence, the temporal evolution of hydrodynamic entropies with $t' = 3t/17, t, t/4$, respectively. In each case, after initial transients, the entropy decreases with time and asymptotes to an approximate constant value.
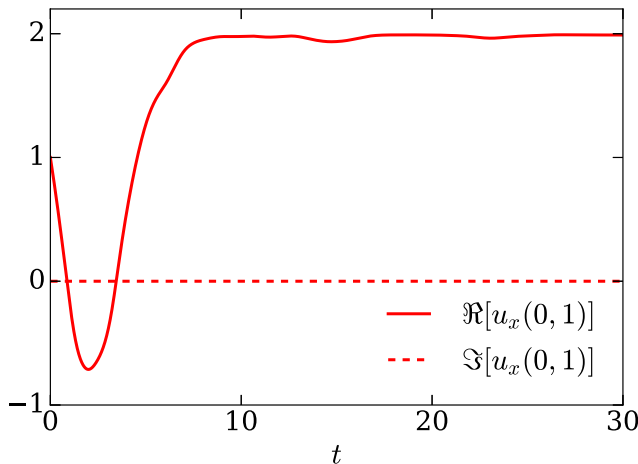
FIG. 10. For run B of 2D Euler turbulence, time series of $\text{Re}[u_x(0, 1)]$ and $\text{Im}[u_x(0, 1)]$. In this run, $\mathbf{u}(0, 1)$ is the most dominant Fourier mode.

the figure, $\text{Im}[u_x(0, 1)] = 0$, while $\text{Re}[u_x(0, 1)]$ approaches nearly a constant value for $t > 10$. The fluctuations in $u_x(0, 1)$ are consistent with those in $T(k, t)$ discussed in Sec. II.

In contrast, for run C, the seven most energetic modes yield an approximate entropy of 2.3, while the rest of them contribute the remaining 0.8. The Fourier modes of run A are more widespread than those of runs B and C, hence run A has the maximum entropy among the three runs. Note that the shear layer of run B has the least entropy, but the vortex-antivortex pair of run A has the maximum entropy, which is still smaller than the maximum possible value of 16.5.

Thus, we show that the hydrodynamic entropy of 2D Euler turbulence decreases with time for a significant duration, even though the system is isolated. Thus, 2D Euler turbulence is a rare isolated system that exhibits evolution from *disorder to order*.

IV. DISCUSSIONS AND CONCLUSIONS

Kraichnan [16] and Onsager [6] assumed that 2D Euler turbulence reaches equilibrium. Kraichnan argued that 2D Euler turbulence exhibits the energy spectrum of Eq. (3), whereas Onsager [6] advocated a large cluster of same-circulation vortices. We performed numerical simulations to test whether 2D Euler turbulence is in equilibrium or out of equilibrium.

Our numerical simulations, as well as several past ones, report that at small wave numbers, the energy spectrum and flux of 2D Euler turbulence differ from those predicted by Kraichnan [16]. These differences arise due to the nonequilibrium nature of 2D Euler turbulence. It is important to note that 2D Euler turbulence is one of the few energy-conserving systems that do not thermalize (or approach equilibrium). Note, however, that several experiments on quantum fluids report consistency with Onsager's theory [7]. Hence, the relationship between Euler turbulence and quantum fluids needs to be examined carefully. We also remark that the flow structures of 2D Euler turbulence do not exhibit long-range order, as in a ferromagnet. Instead, the flow structures resemble vortex-antivortex pairs of Berezinskii-Kosterlitz-Thouless transition [44].

More importantly, we propose hydrodynamic entropy to quantify disorder in Euler turbulence. We observe that the hydrodynamic entropy of 3D Euler turbulence increases monotonically with time, whereas it decreases for 2D Euler turbulence. Thus, 2D Euler turbulence is a unique *isolated* system that exhibits evolution form disorder to order. This feature arises due to the inverse energy cascade, which is a property of 2D hydrodynamics [2,30,32,45]. Hence, the emergence of hydrodynamic order in 2D Euler turbulence has a dynamic origin. Note that the thermodynamic entropy of
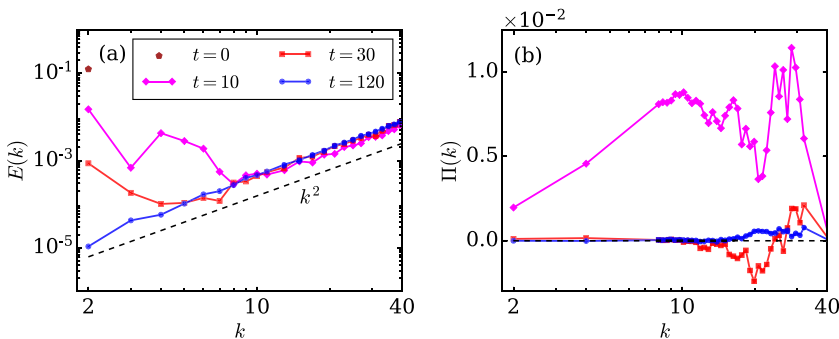
FIG. 11. For 3D Euler turbulence, plots of (a) the energy spectra $E(k)$, and (b) the energy fluxes $\Pi(k)$ at $t = 0, 10, 30, 120$. At $t = 120$, $E(k) \propto k^2$.

Euler turbulence remains constant throughout its evolution. Therefore, *the decrease in hydrodynamic entropy with time does not violate second law of thermodynamics.*

Euler equation is time reversible due to an absence of viscous dissipation [2]. This is the reason why thermodynamic entropy of Euler turbulence is constant [1]. Note, however, that the solutions of Euler equation exhibits irreversibility due to their chaotic and nonequilibrium nature. As we show in this paper, 2D Euler turbulence is a special energy-conserving system that exhibit nonequilibrium behavior. However, 3D Euler turbulence reaches equilibrium asymptotically where detailed balance is preserved statistically [3]. Interestingly, the hydrodynamic entropy captures the irreversibility and disorder of 2D and 3D Euler turbulence quite well.

We conclude this paper by emphasizing that thermal and hydrodynamic processes, with or without viscosity, are multiscale phenomena where hierarchical energy transfers play a critical role [2,34]. Recently, Verma [18,36] attributed irreversibility in a turbulent flow to the asymmetric energy transfers (e.g., forward cascade in 3D Navier-Stokes equation), which is a hydrodynamic property. Following a similar approach, in this paper, we propose hydrodynamic entropy that successfully captures the evolution of 2D Euler turbulence from disorder to order.

APPENDIX: EVOLUTION OF 3D EULER TURBULENCE

In this Appendix, we summarize the energy spectrum and flux of 3D Euler turbulence. Cichowlas *et al.* [3] simulated 3D Euler turbulence with Taylor-Green vortex as an initial condition. For such simulations, in the early phase, the energy flows from large scales to small scales, and the energy flux is positive. After several eddy turnover times, the system approaches equilibrium with vanishing energy flux and $E(k)$ given by Eq. (2).

To compute the hydrodynamic entropy for 3D Euler turbulence, we simulated 3D Euler flow. We performed our simulation on a $(2\pi)^3$ box with a M^3 grid. Here, $M = 128$. We dealiase the code by setting all the modes outside the sphere of radius $M/3$ to zero. We time evolve Eqs. (1) of the main text using PEFRL scheme [25,26] to ensure energy conservation. As in Cichowlas *et al.* [3], we take the Taylor-Green vortex ($k_0 = 1$) as an initial condition, and time evolve the system till 120 eddy turnover time ($2\pi/U_{\text{rms}}$) with a constant $dt = 10^{-4}$. The total energy per unit volume
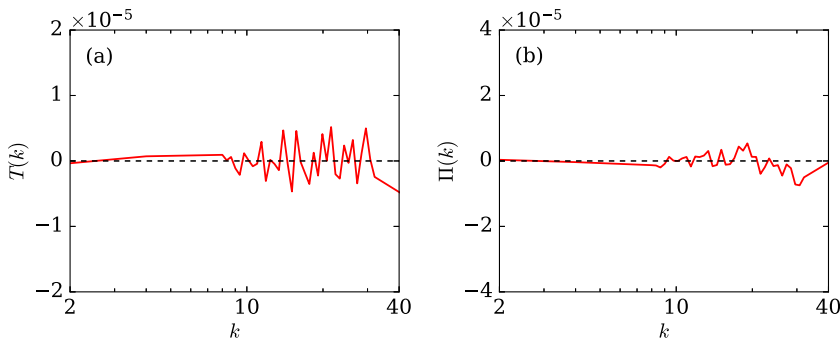
FIG. 12. For 3D Euler turbulence, plots of (a) averaged $T(k, t)$ and (b) averaged $\Pi(k, t)$. We average over 2000 frames in time interval (100, 120).

$E = \int d\mathbf{r}(u^2/2)/\int d\mathbf{r} = 0.125$, and it is conserved up to 12 significant digits till the final time $t = 120$. The system reaches equilibrium in approximately 100 eddy turnover time, consistent with the estimates of Cichowlas *et al.* [3] and Verma *et al.* [19]. In the asymptotic state, the velocity field is δ correlated and it is as random as that in a thermodynamic gas [19]. Using the numerical data, we compute the energy spectrum and flux for the flow at times $t = 0, 10, 30, 120$. For the computation of energy flux, we employ the algorithm outlined in Dar *et al.* [46] and Verma [47]. In Figs. 11(a) and 11(b), we exhibit the energy spectra and energy fluxes at $t = 0, 10, 30, 120$. Clearly, with time, the energy spectrum $E(k)$ spreads from low wave numbers to high wave numbers, and asymptotes to k^2, consistent with the predictions of Kraichnan [16] [Eq. (2) with $\gamma = 0$].

The energy flux is nonzero for the intermediate configurations, but for $t \geqslant 30$, $\Pi(k) \approx 0$ for small k's. Note, however, that $\Pi(k)$ is of the order of 10^{-4} for large wave numbers. The fluctuations in the energy flux are suppressed significantly on averaging over 2000 frames in time interval (100, 120) (see Fig. 12). We expect these fluctuations to subside at a later time when the system has thermalized fully.

We also remark that for the δ-correlated initial velocity profile, $E(k) \propto k^2$ [Eq. (2) with $\gamma = 0$], and energy flux vanishes from the beginning itself [19]. Thus, Euler turbulence remains thermalized throughout for the δ-correlated initial condition.

[1] L. D. Landau and E. M. Lifshitz, *Fluid Mechanics*, 2nd ed., Course of Theoretical Physics (Elsevier, Oxford, 1987)

[2] U. Frisch, *Turbulence: The Legacy of A. N. Kolmogorov* (Cambridge University Press, Cambridge, 1995).

[3] C. Cichowlas, P. Bonaïti, F. Debbasch, and M. E. Brachet, Effective Dissipation and Turbulence in Spectrally Truncated Euler Flows, Phys. Rev. Lett. **95**, 264502 (2005).

[4] D. G. Fox and S. A. Orszag, Inviscid dynamics of two-dimensional turbulence, Phys. Fluids **16**, 169 (1973).

[5] C. E. Seyler, Y. Salu, D. Montgomery, and G. Knorr, Two-dimensional turbulence in inviscid fluids or guiding center plasmas, Phys. Fluids **18**, 803 (1975).

[6] L. Onsager, Statistical hydrodynamics, Il Nuovo Cimento **6**, 279 (1949).

[7] G. Gauthier, M. T. Reeves, X. Yu, A. S. Bradley, M. A. Baker, T. A. Bell, H. Rubinsztein-Dunlop, M. J. Davis, and T. W. Neely, Giant vortex clusters in a two-dimensional quantum fluid, Science **364**, 1264 (2019).

[8] T. P. Billam, M. T. Reeves, B. P. Anderson, and A. S. Bradley, Onsager-Kraichnan Condensation in Decaying Two-Dimensional Quantum Turbulence, Phys. Rev. Lett. **112**, 145301 (2014).

[9] J. Miller, Statistical Mechanics Of Euler Equations in Two Dimensions, Phys. Rev. Lett. **65**, 2137 (1990).

[10] R. Robert, A maximum-entropy principle for two-dimensional perfect fluid dynamics, J. Stat. Phys. **65**, 531 (1991).

[11] F. Bouchet and E. Simonnet, Random Changes of Flow Topology in Two-Dimensional and Geophysical Turbulence, Phys. Rev. Lett. **102**, 094504 (2009).

[12] F. Bouchet and A. Venaille, Statistical mechanics of two-dimensional and geophysical flows, Phys. Rep. **515**, 227 (2012).

[13] R. Pakter and Y. Levin, Nonequilibrium Statistical Mechanics of Two-Dimensional Vortices, Phys. Rev. Lett. **121**, 020602 (2018).

[14] G. L. Eyink and K. R. Sreenivasan, Onsager and the theory of hydrodynamic turbulence, Rev. Mod. Phys. **78**, 87 (2006).

[15] T. D. Lee, On some statistical properties of hydrodynamical and magneto-hydrodynamical fields, Q. Appl. Math. **10**, 69 (1952).

[16] R. H. Kraichnan, Helical turbulence and absolute equilibrium, J. Fluid Mech. **59**, 745 (1973).

[17] R. H. Kraichnan and D. C. Montgomery, Two-dimensional turbulence, Rep. Prog. Phys. **43**, 547 (1980).

[18] M. K. Verma, Boltzmann equation and hydrodynamic equations: Their equilibrium and non-equilibrium behaviour, Phil. Trans. R. Soc. A. **378**, 20190470 (2020).

[19] M. K. Verma, S. Bhattacharya, and S. Chatterjee, Euler turbulence and thermodynamic equilibrium, arXiv:2004.09053 (2020).

[20] G. Joyce and D. Montgomery, Negative temperature states for the two-dimensional guiding-centre plasma, J. Plasma Phys. **10**, 107 (1973).

[21] D. G. Dritschel, W. Qi, and J. B. Marston, On the late-time behaviour of a bounded, inviscid two-dimensional flow, J. Fluid Mech. **783**, 1 (2015).

[22] R. Robert and J. Sommeria, Statistical equilibrium states for two-dimensional flows, J. Fluid Mech. **229**, 291 (1991).

[23] K. Modin and M. Viviani, Canonical scale separation in two-dimensional incompressible hydrodynamics, arXiv:2102.01451.

[24] A. van Kan, A. Alexakis, and M. Brachet, Geometric microcanonical theory of two-dimensional truncated Euler flows, Philos. Trans. R. Soc. A **380**, 20210049 (2022).

[25] I. P. Omelyan, I. M. Mryglod, and R. Folk, Optimized Forest-Ruth- and Suzuki-like algorithms for integration of motion in many-body systems, Comput. Phys. Commun. **146**, 188 (2002).

[26] E. Forest and R. D. Ruth, Fourth-order symplectic integration, Physica D **43**, 105 (1990).

[27] A. Celani, S. Musacchio, and D. Vincenzi, Turbulence in More Than Two and Less than Three Dimensions, Phys. Rev. Lett. **104**, 184506 (2010).

[28] R. Fjørtoft, On the changes in the spectral distribution of kinetic energy for two-dimensional, nondivergent flow, Tellus **5**, 225 (1953).

[29] S. V. Nazarenko, *Wave Turbulence* (Springer-Verlog, Berlin, 2011).

[30] R. H. Kraichnan, Inertial-range transfer in two-and three-dimensional turbulence, J. Fluid Mech. **47**, 525 (1971).

[31] A. J. Majda, Statistical energy conservation principle for inhomogeneous turbulent dynamical systems., Proc. Natl. Acad. Sci. USA **112**, 8937 (2015).

[32] M. K. Verma, *Energy transfers in Fluid Flows: Multiscale and Spectral Perspectives* (Cambridge University Press, Cambridge, 2019).

[33] M. K. Verma, S. Chatterjee, A. Sharma, and A. Mohapatra, Equilibrium states of Burgers and Korteweg–de Vries equations, Phys. Rev. E **105**, 034121 (2022).

[34] M. K. Verma, Variable energy flux in turbulence, J. Phys. A: Math. Theor. **55**, 013002 (2022).

[35] L. D. Landau and E. M. Lifshitz, *Statistical Physics*, 3rd ed., Course of Theoretical Physics (Elsevier, Oxford, 1980).

[36] M. K. Verma, Asymmetric energy transfers in driven nonequilibrium systems and arrow of time, Eur. Phys. J. B **92**, 190 (2019).

[37] P. K. Kundu, I. M. Cohen, and D. R. Dowling, *Fluid Mechanics*, 6th ed. (Academic Press, San Diego, 2015).

[38] A. R. Choudhuri, *Astrophysics for Physicists* (Cambridge University Press, Cambridge, 2010).

[39] C. E. Shannon, A mathematical theory of communication, Bell Labs Tech. J. **27**, 379 (1948).

[40] R. Landauer, Irreversibility and heat generation in the computing process, IBM J. Res. Dev. **44**, 261 (2000).

[41] N. Aubry, R. Guyonnet, and R. Lima, Spatiotemporal analysis of complex signals: Theory and applications, J. Stat. Phys. **64**, 683 (1991).

[42] D. Clark, L. Tarra, and A. Berera, Chaos and information in two-dimensional turbulence, Phys. Rev. Fluids **5**, 064608 (2020).

[43] T. D. Drivas and T. M. Elgindi, Singularity formation in the incompressible Euler equation in finite and infinite time, arXiv:2203.17221.

[44] P. M. Chaikin and T. C. Lubensky, *Principles of Condensed Matter Physics* (Cambridge University Press, New York, 2000).

[45] M. Lesieur, *Turbulence in Fluids* (Springer-Verlag, Dordrecht, 2008).

[46] G. Dar, M. K. Verma, and V. Eswaran, Energy transfer in two-dimensional magnetohydrodynamic turbulence: Formalism and numerical results, Physica D **157**, 207 (2001).

[47] M. K. Verma, Statistical theory of magnetohydrodynamic turbulence: recent results, Phys. Rep. **401**, 229 (2004).